Proceedings of DETC'03
ASME 2003 Design Engineering Technical Conferences and Computers and Information in Engineering Conference
Chicago, ILLINOIS, September 2-6, 2003

DETC2003/DAC-XXXXX

DESIGN SENSITIVITY ANALAYSIS OF NONLINEAR SHELL STRUCTURE WITH FRICTIONLESS CONTACT

Kyung K. Choi and Kiyoung Yi
Center for Computer-Aided Design and
Department of Mechanical & Industrial Engineering
College of Engineering
The University of Iowa
Iowa City, IA 52242, USA
kkchoi@ccad.yiowa.edu,
kyyi@ccad.uiowa.edu

Nam H. Kim
Department of Mechanical & Aerospace Engineering
College of Engineering
University of Florida
Gainesville, FL32611, USA
nkim@ufl.edu

Mark E. Botkin
Vehicle Analysis & Dynamics
General Motors R&D and Planning
Mail Code 480–106–256
30500 Mound Rd. 106
Box 9055
Warren, MI 48090–9055
mark_e._botkin@gmr.com

ABSTRACT

A continuum-based shape and configuration design sensitivity analysis method for a finite deformation elastoplastic shell structure with frictionless contact has been developed. Shell elastoplasticity is treated based on the projection method that performs the return mapping on the subspace defined by the zero-normal stress condition. An incrementally objective integration scheme is used in the context of finite deformation shell analysis, wherein stress objectivity is preserved for finite rotation increments. The penalty regularization method is used to approximate the contact variational inequality. The material derivative concept is used to develop continuum based design sensitivity. The design sensitivity equation is solved without iteration at each converged load step. Numerical implementation of the proposed shape and configuration design sensitivity analysis is carried out using the meshfree method. The accuracy and efficiency of the proposed method is illustrated using numerical examples.

NOMENCLATURE

$a(\bullet,\bullet)$	Structural energy form
$a^*(\bullet,\bullet)$	Linearized structural energy form
$\boldsymbol{\alpha}$	Back stress
β	Hardening parameter
$\boldsymbol{C}^{\text{alg}}$	Global algorithmic tangent tensor
$\boldsymbol{D}^{ep}$	Local elastoplastic algorithmic tangent tensor
$\Delta\boldsymbol{\varepsilon}$	Increments of local strain with dimension 5
$\Delta\boldsymbol{\varepsilon}^l$	Increments of local strain with dimension 9
$\Delta\boldsymbol{\varepsilon}^g$	Increments of global strain with dimension 9
$\bar{e}^p$	Effective plastic strain
$\boldsymbol{F}$	Deformation gradient
H	Hardening parameter
$\boldsymbol{\kappa}$	Radius of yield surface
$\ell(\bullet)$	Load linear form
$\boldsymbol{\sigma}$	Local Cauchy stress with dimension 5
$\boldsymbol{\sigma}^l$	Local Cauchy stress with dimension 9
$\boldsymbol{\sigma}^g$	Global Cauchy stress with dimension 9
$\boldsymbol{s}$	Deviatoric stress
$\Delta\mathbf{z}$	Incremental displacement

1. INTRODUCTION

Shell structures are frequently used in the construction of aerospace, automotive, and civil engineering structures. Most shell components are manufactured by using either stamping or hydroforming processes, which both involve large elastoplastic deformation. A significant amount of effort has been put into the design sensitivity analysis (DSA) and optimization of shell structures [1-5]. Three approaches for DSA were developed for a shell structure: the finite difference method (FDM), the discrete method, and the continuum method. Because FDM is the simplest method, it is frequently

used to optimize shell structures. However it lacks accuracy and involves high computational costs. The discrete method involves differentiation of the approximate matrix equation and has difficulty in obtaining derivatives of numerically constructed stiffness matrices. The continuum method differentiates the variational equation prior to discretization and thus is more efficient and accurate than the previous two methods, although it requires lengthy analytical derivations. In this paper, the design sensitivity formulation of a finite deformation elastoplastic shell structure with frictionless contact has been developed. This paper is the first attempt to apply the continuum DSA method to a large elastoplastic shell structure.

Kim et al. [1] proposed a unified design sensitivity formulation for the linear shell structure using the meshfree method, which is then extended to the nonlinear problem in this paper. Since no element information is generated in the meshfree method, surface information from a CAD tool is necessary for constructing the surface normal vector, and a mapping from the global to local coordinate, both of which are essential in representing the general curved shell structure at the initial configuration. Therefore, the meshfree method can significantly reduce the amount of discretization error that often occurs using the traditional finite element method. In order to account for the finite rotation increment, the normal vector and mapping must be updated using rotational response at the current configuration.

Among several incrementally objective integration schemes in finite deformation analysis, in which stress objectivity is preserved for finite rotation increments, the Hughes-Winget algorithm [6-7] is used in this paper. This algorithm is advantageous for DSA because a formulation of the tangent stiffness matrix that is consistent with other integration scheme is not yet available. In addition, the Hughes-Winget algorithm provides the possibility of using an existing small-strain shell elastoplastic integration procedure without modification.

The most widely used integration procedure for plane strain and three-dimensional elastoplastic analysis is the radial return-mapping algorithm. Since return mapping algorithms are strain driven, three-dimensional return mapping algorithms can be trivially modified for the plane strain problem. Shell elastoplastic integration, however, is non-trivial because of its zero normal stress condition. There have been two approaches: the iterative method with a zero normal stress condition based on the use of the three-dimensional plasticity model, and the projection method, which performs return mapping on the subspace defined by the plane stress condition proposed by Simo and Taylor [8].

In the stamping process, the deformation of the die and the punch are generally ignorable. Therefore, in numerical analysis, the die and punch can be sufficiently modeled as rigid bodies and their discretization is not needed. The rigid-flexible contact algorithm not only saves a significant amount of computational time, it also improves the convergence behavior by providing more accurate contact information such as the contact point, normal vector and so on. In the corresponding DSA, design variables are generally taken as the shape and configuration of the die and punch. Thus, the initial design velocity field is given only at the die and/or punch. However, during the subsequent time step, the design velocity field at the blank sheet is no longer zero and should be updated based on the calculated material derivative of displacement.

The accuracy and efficiency of the proposed method is shown by means of the following numerical examples.

2. RESPONSE ANALYSIS OF FINITE DEFORMATION ELASTOPLASTIC SHELL STRUCTURE

2.1 Shell Elastoplastic Analysis

A brief review of shell elastoplastic analysis is presented to introduce notations that appear in the following DSA section. One complexity in shell elastoplastic analysis is that plastic evolution appears in deviatoric space, while the zero normal stress condition is imposed in stress space. Let V^S be the vector space of symmetric order-2 stress tensors. Thus, $\dim V^S = 6$. The shell stress subspace V^P is obtained from zero normal stress condition as

$$V^P \equiv \left\{ \boldsymbol{\sigma} \in V^S \mid \sigma_{33} = 0 \right\} \tag{1}$$

In addition, the corresponding deviatoric subspace V^D is defined as

$$V^D \equiv \left\{ \boldsymbol{s} \in V^S \mid s_{kk} = 0 \right\} \tag{2}$$

where k is the normal direction. Therefore, $\dim V^P = \dim V^D = 5$. Vector notations are employed to represent each space as

$$\boldsymbol{\sigma} = \left[\sigma_{11} \quad \sigma_{22} \quad \sigma_{12} \quad \sigma_{23} \quad \sigma_{31} \right]^T \tag{3}$$

$$\boldsymbol{s} = \left[s_{11} \quad s_{22} \quad s_{12} \quad s_{23} \quad s_{31} \right]^T \tag{4}$$

Although s_{33} is not included in (4), it is non-zero and can be calculated from the constraint, $s_{kk}=0$. Since the imposition of a zero normal stress constraint is not straightforward in the deviatoric subspace, the mapping relation between $\boldsymbol{\sigma} \in V^P$ and $\boldsymbol{s} \in V^D$ is required. In matrix form it is

$$\boldsymbol{s} = \bar{\boldsymbol{P}}\boldsymbol{\sigma}, \quad \bar{\boldsymbol{P}} = \frac{1}{3}\begin{bmatrix} 2 & -1 & 0 & 0 & 0 \\ -1 & 2 & 0 & 0 & 0 \\ 0 & 0 & 3 & 0 & 0 \\ 0 & 0 & 0 & 3 & 0 \\ 0 & 0 & 0 & 0 & 3 \end{bmatrix} \tag{5}$$

Using the same mapping matrix, the back stress $\boldsymbol{\alpha} \in V^P$ and its deviatoric part $\boldsymbol{\alpha}' \in V^D$ is related by

$$\boldsymbol{\alpha}' = \bar{\boldsymbol{P}}\boldsymbol{\alpha} \tag{6}$$

From small elastic strain and small rigid-body rotation assumptions, the strain and its rate can be additively decomposed into elastic and plastic part as

$$\boldsymbol{\varepsilon} = \boldsymbol{\varepsilon}^e + \boldsymbol{\varepsilon}^p, \qquad \dot{\boldsymbol{\varepsilon}} = \dot{\boldsymbol{\varepsilon}}^e + \dot{\boldsymbol{\varepsilon}}^p \tag{7}$$

Since the vector notations are used to represent the stress, the strains also need to be expressed in vector notation. They have a dimension of five and take the vector form of

$$\begin{aligned} \boldsymbol{\varepsilon} &= \begin{bmatrix} \varepsilon_{11} & \varepsilon_{22} & 2\varepsilon_{12} & 2\varepsilon_{23} & 2\varepsilon_{31} \end{bmatrix}^T \\ \boldsymbol{\varepsilon}^p &= \begin{bmatrix} \varepsilon_{11}^p & \varepsilon_{22}^p & 2\varepsilon_{12}^p & 2\varepsilon_{23}^p & 2\varepsilon_{31}^p \end{bmatrix}^T \end{aligned} \tag{8}$$

The constitutive equation is written

$$\boldsymbol{\sigma} = \boldsymbol{D}\boldsymbol{\varepsilon}^e \tag{9}$$

where $\boldsymbol{D}$ is the elastic constitutive matrix after enforcing zero normal stress constraint.

In rate-independent plasticity, the von Mises yield criterion with an associative flow rule is the well-known method, which is used in this paper. Accordingly, the yield function, is defined as

$$f \equiv \tfrac{1}{2}\boldsymbol{\eta}^T \boldsymbol{P}\boldsymbol{\eta} - \tfrac{1}{3}\kappa^2\left(\bar{e}^p\right) \le 0 \tag{10}$$

where $\boldsymbol{\eta} \equiv \boldsymbol{\sigma} - \boldsymbol{\alpha}$; $\kappa\left(\bar{e}^p\right)$ is the radius of the yield surface, which is determined by the isotropic hardening rule; and where $\boldsymbol{P}$ is the mapping matrix modified from $\bar{\boldsymbol{P}}$ in order to account for the factor of two in the shear strain component, written as

$$\boldsymbol{P} \equiv \frac{1}{3}\begin{bmatrix} 2 & -1 & 0 & 0 & 0 \\ -1 & 2 & 0 & 0 & 0 \\ 0 & 0 & 6 & 0 & 0 \\ 0 & 0 & 0 & 6 & 0 \\ 0 & 0 & 0 & 0 & 6 \end{bmatrix} \tag{11}$$

In what follows, a linearly combined isotropic-kinematic hardening rule is used as

$$\kappa\left(\bar{e}^p\right) = \sigma_0 + \beta H \bar{e}^p \tag{12}$$

where $\bar{e}^p$ is an effective plastic strain; β is one when the pure isotropic hardening rule is used, and zero when the pure kinematic hardening rule is used; σ_0 is the initial yield stress; and H is the hardening parameter. The back stress can be determined by the kinematic hardening rule as

$$\dot{\boldsymbol{\alpha}} = \tfrac{2}{3}\lambda H\left(1-\beta\right)\boldsymbol{\eta} \tag{13}$$

where $\dot{\lambda}$ is a plastic consistency parameter, which is zero when the material is in the elastic status and positive when it is in the plastic status. Since the associative flow rule is used, the plastic strain is proportional to the normal of the yield surface. Thus,

$$\dot{\boldsymbol{\varepsilon}}^p = \dot{\lambda}\boldsymbol{P}\boldsymbol{\eta} \tag{14}$$

The rate of effective strain can be expressed as

$$\dot{\bar{e}}^p = \sqrt{\tfrac{2}{3}}\phi\dot{\lambda} \tag{15}$$

where $\phi = \left[\boldsymbol{\eta}^T \boldsymbol{P}\boldsymbol{\eta}\right]^{1/2}$. Loading/unloading conditions can be formulated using the Kuhn-Tucker condition as

$$f \le 0, \quad \dot{\lambda} \ge 0, \quad \dot{\lambda} f = 0 \tag{16}$$

where the non-positive property of the yield function is regarded as an inequality constraint and the plastic consistency parameter as a corresponding Lagrange multiplier.

2.2 Numerical Integration Procedure

The basic problem of integrating elastoplastic constitutive equations can be stated as follows. On the time interval of interest $[0,T]$, it is assumed that at time t_n the total and plastic strain fields and the back stress field are all known; that is,

$$\left\{ {}^n\boldsymbol{\varepsilon},\ {}^n\boldsymbol{\varepsilon}^p,\ {}^n\bar{e}^p,\ {}^n\boldsymbol{\alpha} \right\} \text{ are known fields at time } t_n \tag{17}$$

In the displacement-driven solution procedure, the incremental displacement field over the time step $[t_n, t_{n+1}]$ is available, from which the incremental strain $\Delta\boldsymbol{\varepsilon}$ can be calculated. From additive decomposition, the strain at time t_n can be calculated by

$${}^{n+1}\boldsymbol{\varepsilon} = {}^n\boldsymbol{\varepsilon} + \Delta\boldsymbol{\varepsilon} \tag{18}$$

The remaining independent variables must be updated using the integration algorithm. A standard backward Euler method is used to integrate the rate-form elastoplastic equations. First, it is assumed that the incremental strain is elastic, which means that all plastic variables remain fixed. Using the subscript "tr" to denote the trial status, the following relations are obtained:

$$\begin{cases} \boldsymbol{\varepsilon}_{tr}^p = {}^n\boldsymbol{\varepsilon}^p \\ \boldsymbol{\alpha}_{tr} = {}^n\boldsymbol{\alpha} \\ \bar{e}_{tr}^p = {}^n e^p \\ \boldsymbol{\sigma}_{tr} = \boldsymbol{D}\left({}^{n+1}\boldsymbol{\varepsilon} - {}^n\boldsymbol{\varepsilon}\right) \\ \boldsymbol{\eta}_{tr} = \boldsymbol{\sigma}_{tr} - \boldsymbol{\alpha}_{tr} \end{cases} \tag{19}$$

Using this trial status, the yield function in equation (10) is evaluated. If $f \le 0$, then the trial status is the final status and the material is in the elastic range. Otherwise, the material is in the plastic range, and return mapping is performed, to find the non-negative consistency parameter λ_{n+1},which makes the yield function vanish, i.e., $f(\lambda_{n+1})=0$. The backward Euler

integration algorithm of the rate-form evolution equations can be written as

$$\begin{cases} {}^{n+1}\boldsymbol{\varepsilon}^p = {}^{n}\boldsymbol{\varepsilon}^p + {}^{n+1}\lambda \boldsymbol{P}\, {}^{n+1}\boldsymbol{\eta} \\ {}^{n+1}\boldsymbol{\alpha} = {}^{n}\boldsymbol{\alpha} + {}^{n+1}\lambda \tfrac{2}{3}(1-\beta) H\, {}^{n+1}\boldsymbol{\eta} \\ {}^{n+1}\overline{e}^{\,p} = {}^{n}\overline{e}^{\,p} + {}^{n+1}\lambda \sqrt{\tfrac{2}{3}}\, {}^{n+1}\phi \\ {}^{n+1}\boldsymbol{\sigma} = \boldsymbol{D}\left({}^{n+1}\boldsymbol{\varepsilon} - {}^{n+1}\boldsymbol{\varepsilon}^p \right) \\ {}^{n+1}\boldsymbol{\eta} = {}^{n+1}\boldsymbol{\sigma} - {}^{n+1}\boldsymbol{\alpha} \end{cases} \tag{20}$$

The plastic consistency parameter λ_{n+1} is obtained by enforcing the plastic consistency condition at t_n. After inserting the relations in the above equation into equation (10) , the consistency condition is written, in the form

$${}^{n+1}\phi = \sqrt{\tfrac{2}{3}}\left[{}^{0}\sigma + \beta H\, {}^{n}\overline{e}^{\,p} \right] + \tfrac{2}{3}\beta H\, {}^{n+1}\lambda\, {}^{n+1}\phi \tag{21}$$

The above equation is a nonlinear algebraic equation, which is solved using the Newton-Raphson iterative method. After solving λ_{n+1} from equation (21), all independent variables in equation (20) are updated at time t. The integration algorithm in equation (20) preserves the zero normal stress condition.

2.3 Finite Deformation Shell Analysis

Although there are several incrementally objective integration schemes, they can be cast into a uniform format, form-identical to small-deformation theory. They take on canonically simple forms when transformed to rotation-free configuration. Therefore, the way in which finite incremental rotation is evaluated the key difference between these schemes. Among the several incrementally objective integration schemes, the Hughes-Winget algorithm is used in this paper, summarized as follows:

$${}^{n+1}\sigma_{ij}^{g} = r_{ik}\, {}^{n}\sigma^{g} r_{jl} + \Delta\sigma_{ij}^{g} \tag{22}$$

where the second term represents the material response and is determined by the numerical integration procedure presented in the previous section, whereas the first term accounts for rotational effects, and where r_{ij} is defined using the midpoint rule as

$$r_{ij} = \delta_{ij} + \left(\delta_{ik} - \tfrac{1}{2}\Delta\omega_{ik} \right)^{-1} \Delta\omega_{kj} \tag{23}$$

If the global stress vector is defined as

$$\boldsymbol{\sigma}^{g} \equiv \left[\sigma_{11}\ \ \sigma_{12}\ \ \sigma_{13}\ \ \sigma_{21}\ \ \sigma_{22}\ \ \sigma_{23}\ \ \sigma_{31}\ \ \sigma_{32}\ \ \sigma_{33} \right]^{T} \tag{24}$$

the equation (22) can be written with vector notation as

$${}^{n+1}\boldsymbol{\sigma}^{g} = \boldsymbol{R}\, {}^{n}\boldsymbol{\sigma}^{g} + \Delta\boldsymbol{\sigma}^{g} \tag{25}$$

where $\boldsymbol{R}$ is the 9×9 rotational matrix defined as $R_{ijkl} = r_{ik} r_{jl}$. The key advantage of the Hughes-Winget algorithm is the ability to use the small deformation integration procedure introduced in the previous section where the stress vector is defined in the body-fixed local coordinate. Global stress can be transformed to local stress by using the 9×9 transformation matrix as

$${}^{n+1}\boldsymbol{\sigma}^{l} = {}^{n+1}\boldsymbol{Q}\, {}^{n+1}\boldsymbol{\sigma}^{g}, \qquad {}^{n+1}\boldsymbol{\sigma}^{g} = {}^{n+1}\boldsymbol{Q}^{T}\, {}^{n+1}\boldsymbol{\sigma}^{l} \tag{26}$$

and the transformation matrix at the current configuration must be updated consistently with the finite deformation integration algorithm as

$${}^{n+1}\boldsymbol{Q}^{T} = \boldsymbol{R}\, {}^{n}\boldsymbol{Q}^{T}, \qquad {}^{n+1}\boldsymbol{Q} = {}^{n}\boldsymbol{Q}\boldsymbol{R}^{T} \tag{27}$$

The strain and rotational increments are calculated at the midpoint configuration to maintain the second-order accuracy as

$$\Delta\varepsilon_{ij}^{g} = \tfrac{1}{2}\left(\Delta z_{\,i,\,{}^{n+\frac{1}{2}}x_j} + \Delta z_{\,j,\,{}^{n+\frac{1}{2}}x_i} \right) \tag{28}$$

$$\Delta\omega_{ij} = \tfrac{1}{2}\left(\Delta z_{\,i,\,{}^{n+\frac{1}{2}}x_j} - \Delta z_{\,j,\,{}^{n+\frac{1}{2}}x_i} \right) \tag{29}$$

where ${}^{n+1}\boldsymbol{x} = {}^{0}\boldsymbol{x} + {}^{n+1}\boldsymbol{z}$ and ${}^{n+1}\boldsymbol{x} = {}^{n}\boldsymbol{x} + \Delta\boldsymbol{z}$.

Since the strain increment is evaluated at the midpoint, it needs to be rotated to midpoint configuration as

$$\Delta\boldsymbol{\varepsilon}^{l} = {}^{n}\boldsymbol{Q}^{\frac{1}{2}}\boldsymbol{R}\Delta\boldsymbol{\varepsilon}^{g} \tag{30}$$

The rotation matrix ${}^{\frac{1}{2}}\boldsymbol{R}$ is approximated with half displacement as ${}^{\frac{1}{2}}R_{ijkl} = {}^{\frac{1}{2}}r_{ik}\, {}^{\frac{1}{2}}r_{jl}$ where

$${}^{\frac{1}{2}}r_{ij} \cong \delta_{ij} + \tfrac{1}{2}\left(\delta_{ik} - \tfrac{1}{4}\Delta\omega_{ik} \right)^{-1} \Delta\omega_{kj} \tag{31}$$

Despite the fact that this approximation does not satisfy the condition $\boldsymbol{r} = {}^{\frac{1}{2}}\boldsymbol{r}\, {}^{\frac{1}{2}}\boldsymbol{r}$, the error is second order and its material derivative is much simpler than the exact one.

2.4 Variational Principle

If we let the structural domain at current time t_{n+1} be ${}^{n+1}\Omega$ and previous time t_n be ${}^{n}\Omega$, then the structural energy form at the current configuration is written as

$$\begin{aligned} a\left({}^{n+1}\boldsymbol{z}, \overline{\boldsymbol{z}} \right) &= \iiint_{{}^{n+1}\Omega} \overline{z}_{\,i,\,{}^{n+1}x_j}\, {}^{n+1}\sigma_{ij}\, d\Omega \\ &= \iiint_{{}^{n}\Omega} \overline{z}_{\,i,\,{}^{n}x_m} F_{mj}^{-1}\, {}^{n+1}\sigma_{ij} J d\Omega \end{aligned} \tag{32}$$

where $\overline{\boldsymbol{z}}$ denotes the displacement variation or the virtual displacement, F_{ij} is the deformation gradient defined as $F_{ij}=\partial^{n+1}x_i/\partial^{n}x_j$, and $\boldsymbol{J}$ is the Jacobian between configurations t_n and t_{n+1}.

If a conservative system were considered, then the external force would be independent of deformation. If we let f^B be the body force per unit volume, then the load linear form can be written as

$$l(\bar{z}) = \iiint_{^{n+1}\Omega} \bar{z}_i f_i^B d\Omega = \iiint_{^{n}\Omega} \bar{z}_i f_i^B J d\Omega \tag{33}$$

By equating equations (32) and (33), the variational equation for the nonlinear shell structure is obtained as

$$a\left({}^{n+1}\boldsymbol{z}, \bar{\boldsymbol{z}}\right) = l\left(\bar{\boldsymbol{z}}\right), \quad \text{for all } \bar{\boldsymbol{z}} \in Z \tag{34}$$

where

$$Z = \left\{ \boldsymbol{z} \in \left[H^1(\Omega) \right]^3 \mid \boldsymbol{z}(\boldsymbol{x}) = 0, \ \boldsymbol{x} \in \Gamma_g \right\} \tag{35}$$

is the space of kinematically admissible displacements, $H^l(\Omega)$ is first-order Sobolev space, and Γ_g is the essential boundary where the displacement is prescribed.

The nonlinear equation (34) can be solved using a Newton iterative method through linearization. The linearized equation is

$$a^*\left({}^{n+1}\boldsymbol{z}^k; \Delta\boldsymbol{z}^{k+1}, \bar{\boldsymbol{z}}\right) = l\left(\bar{\boldsymbol{z}}\right) - a\left({}^{n+1}\boldsymbol{z}^k, \bar{\boldsymbol{z}}\right) \tag{36}$$

For a given load step, equation (36) is solved iteratively until the right hand side (residual force) vanishes. The expression of $a^*\left({}^{n+1}\boldsymbol{z}^k; \Delta\boldsymbol{z}^{k+1}, \bar{\boldsymbol{z}}\right)$ will be derived in the next section for DSA

3. DESIGN SENSITIVITY ANALYSIS OF FINITE DEFORMATION ELASTPOPLASTIC SHELL

The material derivative of the load linear form can be carried out to obtain

$$\left.\frac{d}{d\tau} l(\bar{z})\right|_{\tau=0} = \iiint_{^{n}\Omega} \left(\bar{z}_i f_i^B div\, {}^{n}V \right) J d\Omega \equiv l'(\bar{z}) \tag{37}$$

where the force is assumed to be independent of the design; that is, $\left(\boldsymbol{f}^B\right)' = 0$. If a concentrated, constant load is applied to the structure, then the material derivative in equation (37) vanishes. The material derivative of the structural form can be obtained as

$$\begin{aligned} &\left.\frac{d}{d\tau}\left[a\left({}^{n+1}\boldsymbol{z}, \bar{\boldsymbol{z}}\right)\right]\right|_{\tau=0} = \\ &\iiint_{^{n}\Omega}\Big[\left(\bar{z}_{i,{}^{n}x_m}\right)^{\cdot} F_{mj}^{-1\ n+1}\sigma_{ij}^g J + \bar{z}_{i,{}^{n}x_m} \dot{F}_{mj}^{-1\ n+1}\sigma_{ij}^g J \\ &\quad + \bar{z}_{i,{}^{n}x_m} F_{mj}^{-1\ n+1}\dot{\sigma}_{ij}^g J + \bar{z}_{i,{}^{n}x_m} F_{mj}^{-1\ n+1}\sigma_{ij}^g J^{\cdot} \\ &\quad + \bar{z}_{i,{}^{n}x_m} F_{mj}^{-1\ n+1}\sigma_{ij}^g div\, {}^{n}V J \Big] d\Omega \end{aligned} \tag{38}$$

The material derivative of the gradient of the virtual displacement with respect to the position vector at the previous configuration can be found in Haug, et al, [9] as

$$\left(\bar{z}_{i,{}^{n}x_m}\right)^{\cdot} = -\bar{z}_{i,{}^{n}x_k}\, {}^{n}V_{k,{}^{n}x_m} \tag{39}$$

Define $\varepsilon_{im}^V(\bar{z})$ as the multiplication of the above term with the deformation gradient as

$$\varepsilon_{im}^V(\bar{z}) \equiv \left(\bar{z}_{i,{}^{n}x_m}\right)^{\cdot} F_{mj}^{-1} = -\bar{z}_{i,{}^{n}x_k}\, {}^{n}V_{k,{}^{n}x_m} F_{mj}^{-1} \tag{40}$$

The material derivative of the inverse of the deformation gradient and the Jacobian are obtained by exploiting well-known kinematic relations as

$$\dot{F}_{mj}^{-1} = -F_{ml}^{-1}\Delta\dot{z}_{l,{}^{n+1}x_j}, \quad \dot{J} = J\Delta\dot{z}_{k,{}^{n+1}x_k} \tag{41}$$

Since the elastoplastic integration is performed with local stress, the material derivative of global stress needs to be derived from the local stress and transformation matrix as

$${}^{n+1}\dot{\boldsymbol{\sigma}}^g = {}^{n+1}\dot{\boldsymbol{Q}}^T\, {}^{n+1}\boldsymbol{\sigma}^l + {}^{n+1}\boldsymbol{Q}^T\, {}^{n+1}\dot{\boldsymbol{\sigma}}^l \tag{42}$$

The material derivative of local stress can be obtained from the constitutive relation in equation (20), which can be summarized as

$${}^{n+1}\boldsymbol{\sigma} = {}^{n}\boldsymbol{\sigma} + \boldsymbol{D}\Delta\boldsymbol{\varepsilon} - \lambda\boldsymbol{D}\boldsymbol{P}\, {}^{n+1}\boldsymbol{\eta} \tag{43}$$

and its material derivative as

$${}^{n+1}\dot{\boldsymbol{\sigma}} = {}^{n}\dot{\boldsymbol{\sigma}} + \boldsymbol{D}\Delta\dot{\boldsymbol{\varepsilon}} - \dot{\lambda}\boldsymbol{D}\boldsymbol{P}\, {}^{n+1}\boldsymbol{\eta} - \lambda\boldsymbol{D}\boldsymbol{P}\left({}^{n+1}\dot{\boldsymbol{\sigma}} - {}^{n+1}\dot{\boldsymbol{\alpha}}\right) \tag{44}$$

Note that the matrices $\boldsymbol{D}$ and $\boldsymbol{P}$ are independent of design variables. The right-hand side includes ${}^{n}\dot{\boldsymbol{\sigma}}$, which is computed at the previous time step; $\Delta\dot{\boldsymbol{\varepsilon}}$, which is a function of the unknown $\dot{\boldsymbol{z}}$; and ${}^{n+1}\dot{\boldsymbol{a}}$ and $\dot{\lambda}$, which are to be obtained from shell elastoplastic equations. The material derivative of back stress can be obtained from the second equation in (20) as

$${}^{n+1}\dot{\boldsymbol{\alpha}} = \frac{1}{f_1}\, {}^{n}\dot{\boldsymbol{\alpha}} + \frac{f_1'}{f_1}\left(\dot{\lambda}\, {}^{n+1}\boldsymbol{\eta} + \lambda\, {}^{n+1}\dot{\boldsymbol{\sigma}}\right) \tag{45}$$

where $f_1 = 1 + \frac{2}{3}\lambda H(1-\beta)$ and $f_1' = \frac{2}{3}H(1-\beta)$.

The material derivative of plastic consistency parameter λ can be obtained from the consistency condition in equation (21) as

$$\dot{\lambda} = \frac{\left(1 - \frac{2}{3}\beta H\lambda\right)}{\frac{2}{3}H\, {}^{n+1}\phi^2}\left[{}^{n+1}\boldsymbol{\eta}^T\boldsymbol{P}\, {}^{n+1}\dot{\boldsymbol{\sigma}} - {}^{n+1}\boldsymbol{\eta}^T\boldsymbol{P}\, {}^{n}\boldsymbol{\alpha}\right] - \frac{\sqrt{\frac{3}{2}}\beta f_1}{{}^{n+1}\phi}\, {}^{n}\dot{\bar{e}}^p \tag{46}$$

Inserting equation (45) and (46) into equation (44) and defining $f_2 = \frac{2}{3}H\, {}^{n+1}\phi^2 + \left(1 - \frac{2}{3}\beta H\lambda\right) {}^{n+1}\boldsymbol{\eta}^T\boldsymbol{P}\boldsymbol{\Xi}\boldsymbol{D}\boldsymbol{P}\, {}^{n+1}\boldsymbol{\eta}$, $f_3 = f_1\left(1 - \frac{2}{3}\beta H\lambda\right)/f_2$, and $\boldsymbol{\Xi} = \left[f_1\boldsymbol{I} + \lambda\boldsymbol{D}\boldsymbol{P}\right]^{-1}$ yields the final expression for the material derivative of local stress as

$${}^{n+1}\dot{\boldsymbol{\sigma}} = \boldsymbol{D}^{ep}\Delta\dot{\boldsymbol{\varepsilon}} + \boldsymbol{\sigma}^{fic\_l} \tag{47}$$

where

$$\boldsymbol{D}^{ep} = \begin{cases} \boldsymbol{D} & (elastic) \\ f_1 \boldsymbol{\Xi D} - f_3 \boldsymbol{\Xi D P}^{n+1}\boldsymbol{\eta}^{n+1}\boldsymbol{\eta}^T \boldsymbol{P D \Xi} & (plastic) \end{cases} \tag{48}$$

$$\boldsymbol{\sigma}^{fic\_l} = \begin{cases} {}^{n}\dot{\boldsymbol{\sigma}}^{l} & (elastic) \\ \left[f_1 \boldsymbol{\Xi} - f_3 \boldsymbol{\Xi D P}^{n+1}\boldsymbol{\eta}^{n+1}\boldsymbol{\eta}^T \boldsymbol{P \Xi} \right] {}^{n}\dot{\boldsymbol{\sigma}}^{l} + \\ \left[\lambda \boldsymbol{\Xi D P} - f_3 \lambda \boldsymbol{\Xi D P}^{n+1}\boldsymbol{\eta}^{n+1}\boldsymbol{\eta}^T \boldsymbol{P \Xi D P} \right. \\ \qquad \left. + f_3 \lambda \boldsymbol{\Xi D P}^{n+1}\boldsymbol{\eta}^{n+1}\boldsymbol{\eta}^T \boldsymbol{P} \right] {}^{n}\dot{\boldsymbol{\alpha}} + \\ \dfrac{f_1 \sqrt{\frac{2}{3}} \beta H \phi}{f_2} \boldsymbol{\Xi D P}^{n+1}\boldsymbol{\eta}\, {}^{n}\dot{\bar{e}}^{p} & (plastic) \end{cases} \tag{49}$$

For a small deformation problem, the sensitivity equation can be set up by inserting equations (42) and (47) into the material derivative of structural form in equation (38) and equating it with the material derivative of load linear form in equation (37) with small deformation assumptions ${}^{n+1}\boldsymbol{Q} = {}^{n}\boldsymbol{Q}$, $\boldsymbol{F} = \boldsymbol{I}$.

In order to extend the sensitivity equation to the finite deformation problem, material derivatives of rotation matrices in the stain increment as in (30) and in the global-to-local transformation matrix as in (27) must be considered as

$$\Delta\dot{\boldsymbol{\varepsilon}}^{l} = {}^{n}\dot{\boldsymbol{Q}}^{\frac{1}{2}}\boldsymbol{R}^T \Delta\boldsymbol{\varepsilon}^{g} + {}^{n}\boldsymbol{Q}^{\frac{1}{2}}\dot{\boldsymbol{R}}^T \Delta\boldsymbol{\varepsilon}^{g} + {}^{n}\boldsymbol{Q}^{\frac{1}{2}}\boldsymbol{R}^T \Delta\dot{\boldsymbol{\varepsilon}}^{g} \tag{50}$$

$${}^{n+1}\dot{\boldsymbol{Q}}^{T\ n+1}\boldsymbol{\sigma} = \dot{\boldsymbol{R}}\, {}^{n}\boldsymbol{Q}^{T\ n+1}\boldsymbol{\sigma} + \boldsymbol{R}\, {}^{n}\dot{\boldsymbol{Q}}^{T\ n+1}\boldsymbol{\sigma} \tag{51}$$

For notational simplicity, the following relations are used

$${}^{\frac{1}{2}}\dot{\boldsymbol{R}}^T \Delta\boldsymbol{\varepsilon}^{g} = \boldsymbol{A}^{\varepsilon\ \frac{1}{2}}\dot{\boldsymbol{r}}, \quad \dot{\boldsymbol{R}}\boldsymbol{Q}^{T\ n+1}\boldsymbol{\sigma} = \boldsymbol{A}^{\sigma}\dot{\boldsymbol{r}} \tag{52}$$

where

$$\begin{aligned} A^{\varepsilon}_{ijkl} &= \left(\delta_{km}\delta_{in}r_{lj} + \delta_{lm}\delta_{nj}r_{ki} \right) \Delta\varepsilon^{g}_{kl} \\ A^{\sigma}_{ijkl} &= \left(\delta_{im}\delta_{kn}r_{jl} + \delta_{jm}\delta_{nl}r_{ik} \right) {}^{n}Q_{pqkl}\ {}^{n+1}\sigma_{pq} \end{aligned} \tag{53}$$

Taking the material derivative of equations (23) and (31) yields

$$\dot{\boldsymbol{r}} = \boldsymbol{B}^{\sigma}\Delta\dot{\boldsymbol{\omega}}, \qquad {}^{\frac{1}{2}}\dot{\boldsymbol{r}} = \boldsymbol{B}^{\varepsilon}\Delta\dot{\boldsymbol{\omega}} \tag{54}$$

where

$$\begin{aligned} B^{\varepsilon}_{ijkl} &= \left(4\delta_{ik} - \Delta\omega_{ik} \right)^{-1} \left(\delta_{lj} + r_{lj} \right) \\ B^{\sigma}_{ijkl} &= \left(2\delta_{ik} - \Delta\omega_{ik} \right)^{-1} \left(\delta_{lj} + r_{lj} \right) \end{aligned} \tag{55}$$

The remaining steps in the procedure involve taking the material derivative of $\Delta\varepsilon^{g}_{ij}$ and $\Delta\omega_{ij}$ consistently with the midpoint rule. Both terms contain the material derivative of the gradient of the displacement increment with respect to the position vector at the midpoint configuration. Their material derivative thus becomes

$$\begin{aligned} \left(\Delta z_{i,\ {}^{n+\frac{1}{2}}x_j} \right)^{\cdot} &= M_{ijkl} \left(\Delta z_{k,\ {}^{n}x_p} \right)^{\cdot}\ {}^{n}x_{p,\ {}^{n+1}x_l} \\ &= M_{ijkl} \left[\Delta\dot{z}_{i,\ {}^{n+1}x_j} + \varepsilon^{V}_{kl}\left(\Delta z \right) \right] \end{aligned} \tag{56}$$

where

$$M_{ijkl} = {}^{n}x_{i,\ {}^{n+\frac{1}{2}}x_k}\ {}^{n+1}x_{l,\ {}^{n+\frac{1}{2}}x_j} \tag{57}$$

A detailed derivation of M_{ijkl} can be found in the literature by Fish and Shek [10]. By dividing the material derivative of $\Delta\varepsilon^{g}_{ij}$ and $\Delta\omega_{ij}$ into symmetric and antisymmetric parts, it can be expressed as

$$\begin{aligned} \Delta\dot{\varepsilon}_{ij} &= M_{(ij)kl} \left[\Delta\dot{z}_{i,\ {}^{n+1}x_j} + \varepsilon^{V}_{kl}\left(\Delta z \right) \right] \\ \Delta\dot{\omega}_{ij} &= M_{[ij]kl} \left[\Delta\dot{z}_{i,\ {}^{n+1}x_j} + \varepsilon^{V}_{kl}\left(\Delta z \right) \right] \end{aligned} \tag{58}$$

Define $\Delta\dot{z}_{i,\ {}^{n+1}x_j} \equiv \dot{v}_{i,\ {}^{n+1}x_j}$ for notational convenience. The final expression for the material derivative of global stress is obtained by inserting equations (47), (50), (51), and (58) into (42) as

$${}^{n+1}\dot{\boldsymbol{\sigma}}^{g} = \boldsymbol{C}^{\mathrm{alg}}\dot{\boldsymbol{v}} + \boldsymbol{\sigma}^{fic\_g} \tag{59}$$

where

$$\begin{aligned} \boldsymbol{C}^{\mathrm{alg}} = \Big[& \boldsymbol{A}^{\sigma}\boldsymbol{B}^{\sigma}\hat{\boldsymbol{M}} \\ & + {}^{n+1}\boldsymbol{Q}^T \boldsymbol{D}^{p}\, {}^{n}\boldsymbol{Q}\boldsymbol{A}^{\varepsilon}\boldsymbol{B}^{\varepsilon}\hat{\boldsymbol{M}} + {}^{n+1}\boldsymbol{Q}^T \boldsymbol{D}^{p}\, {}^{n+\frac{1}{2}}\boldsymbol{Q}\tilde{\boldsymbol{M}} \Big] \end{aligned} \tag{60}$$

$$\begin{aligned} \boldsymbol{\sigma}^{fic\_g} = & \boldsymbol{R}\, {}^{n}\boldsymbol{Q}^{T\ n+1}\boldsymbol{\sigma} \\ & + {}^{n+1}\boldsymbol{Q}^T \boldsymbol{D}^{ep}\, {}^{n}\dot{\boldsymbol{Q}}^{\frac{1}{2}}\boldsymbol{R}^T \Delta\boldsymbol{\varepsilon}^{g} + {}^{n+1}\boldsymbol{Q}^T \boldsymbol{\sigma}^{fic\_l} \end{aligned} \tag{61}$$

By using the relations in (39), (41), and (59), the material derivative of the structural energy form becomes

$$\frac{d}{d\tau}\Big[a\left({}^{n+1}\boldsymbol{z}, \bar{\boldsymbol{z}} \right) \Big]\Big|_{\tau=0} = a^{*}\left({}^{n+1}\boldsymbol{z}; \Delta\dot{\boldsymbol{z}}, \bar{\boldsymbol{z}} \right) + a'_{V}\left({}^{n+1}\boldsymbol{z}, \bar{\boldsymbol{z}} \right) \tag{62}$$

where

$$\begin{aligned} & a^{*}\left({}^{n+1}\boldsymbol{z}; \Delta\dot{\boldsymbol{z}}, \bar{\boldsymbol{z}} \right) = \\ & \iiint_{{}^{n+1}\Omega} \bar{z}_{i,x_j} \left[C^{\mathrm{alg}}_{ijkl} + \delta_{kl}\sigma^{g}_{ij} - \delta_{kj}\sigma_{il} \right] \Delta\dot{z}_{k,x_l}\, d\Omega \end{aligned} \tag{63}$$

is in the same form as the linearized structural energy form if $\Delta\boldsymbol{z}$ is substituted into $\Delta\dot{\boldsymbol{z}}$. In addition,

$$\begin{aligned} & a'_{V}\left(\boldsymbol{z}, \bar{\boldsymbol{z}} \right) \equiv \\ & \iiint_{{}^{n+1}\Omega} \Big[\varepsilon^{V}_{ij}\left(\bar{\boldsymbol{z}} \right)\sigma^{g}_{ij} + \bar{z}_{i,x_j} C^{\mathrm{alg}}_{ijkl}\varepsilon^{V}_{ij}\left(\Delta\boldsymbol{z} \right) \\ & \qquad + \bar{z}_{i,x_j}\sigma^{fic\_g}_{ij} + \bar{z}_{i,x_j}\sigma^{g}_{ij}\, div\, {}^{n}\boldsymbol{V} \Big] d\Omega \end{aligned} \tag{64}$$

is the structural fictitious load form, which explicitly depends on the design velocity field ${}^{n}V$. After a converged solution is obtained at t_{n+1}, equation (64) is computed using the given design velocity field. By combining equations (37) and (62), the material derivative of the variational equation is obtained as

$$a^*\left({}^{n+1}\boldsymbol{z};\Delta\dot{\boldsymbol{z}},\overline{\boldsymbol{z}}\right)=l'_V\left(\overline{\boldsymbol{z}}\right)-a'_V\left({}^{n+1}\boldsymbol{z},\overline{\boldsymbol{z}}\right) \tag{65}$$

which is solved using the already decomposed tangent stiffness matrix at the converged configuration with a different fictitious load for each shape design variable. Although analysis requires an iterative method, the sensitivity equation in (65) is solved without iteration since $a^*\left({}^{n+1}\boldsymbol{z};\Delta\dot{\boldsymbol{z}},\overline{\boldsymbol{z}}\right)$ is form-identical in nonlinear analysis.

4. FRICTIONLESS CONTACT PROBLEM

4.1 Response Analysis of Frictionless Contact Problem

This section deals with a contact problem between a blank sheet, that experience large elastoplastic deformation, and rigid die and punch. Figure 1 illustrates the contact situation between master and slave body. A blank sheet is referred to as the slave body and the die and punch are referred to as the master body. The master surface is represented by the two parameters in CAD geometric surface information as $\boldsymbol{x}^c(\xi_1,\xi_2)$. Therefore, two tangential vectors and a normal vector on the master surface are defined as

$$\boldsymbol{e}_1=\boldsymbol{x}^c_{,1},\quad \boldsymbol{e}_2=\boldsymbol{x}^c_{,2},\quad \boldsymbol{n}=\boldsymbol{e}_1\times\boldsymbol{e}_2/\left\|\boldsymbol{e}_1\times\boldsymbol{e}_2\right\| \tag{66}$$

where $\boldsymbol{x}_{,\alpha}=\partial\boldsymbol{x}/\partial\xi_\alpha$, α=1,2. The contact point $\boldsymbol{x}^c\in\Gamma_x^2$ corresponding to the slave point $\boldsymbol{x}\in\Gamma_x^1$ is determined from the following consistency condition:

$$\boldsymbol{e}_\alpha\cdot\left(\boldsymbol{x}-\boldsymbol{x}^c\right)=0,\quad \alpha=1,2 \tag{67}$$

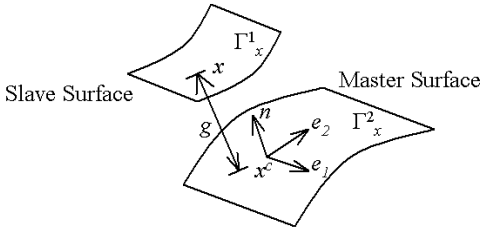

Figure 1. Contact kinematics

Note that $\boldsymbol{x}^c$ is the closest projection point of $\boldsymbol{x}$. Using the normal gap function, which is the normal distance between two bodies, the impenetrability condition can be imposed as

$$g=\boldsymbol{n}\cdot\left(\boldsymbol{x}-\boldsymbol{x}^c\right)\geq 0 \tag{68}$$

The violated region Γ^c of the constraint in equation (68) is penalized using a penalty function, which is defined as

$$P=\frac{1}{2}\omega_n\int_{\Gamma^c}g^2d\Gamma \tag{69}$$

where ω_n is the penalty parameter. The variation of the penalty function becomes the contact variational form, which is defined as

$$b_N\left({}^{n+1}\boldsymbol{z},\overline{\boldsymbol{z}}\right)\equiv\overline{P}=\omega_n\int_{\Gamma^c}g\overline{g}d\Gamma \tag{70}$$

where $\omega_n g$ corresponds to the compressive normal force. The variation of the gap function is obtained from its definition as $\overline{g}=\boldsymbol{n}\cdot\overline{\boldsymbol{z}}$. Note that the variation of master surface displacement $\overline{\boldsymbol{z}}^c$ vanishes, since the master body is assumed to be rigid. I addition, the variation of the normal vector vanishes due to the orthogonal condition.

By combining equation (70) with (34), the approximated variational equation for the penalized contact condition becomes

$$a\left({}^{n+1}\boldsymbol{z},\overline{\boldsymbol{z}}\right)+b_N\left({}^{n+1}\boldsymbol{z},\overline{\boldsymbol{z}}\right)=l\left(\overline{\boldsymbol{z}}\right),\qquad\forall\overline{\boldsymbol{z}}\in Z \tag{71}$$

Note that even if the structure undergoes an elastic process, equation (71) is nonlinear since the inequality constraint is imposed throughout the penalty method. The corresponding linearized incremental equation is

$$\begin{aligned}a^*\left({}^{n+1}\boldsymbol{z}^k;\Delta\boldsymbol{z}^{k+1},\overline{\boldsymbol{z}}\right)+b_N^*\left({}^{n+1}\boldsymbol{z}^k;\Delta\boldsymbol{z}^{k+1},\overline{\boldsymbol{z}}\right)=\\ l\left(\overline{\boldsymbol{z}}\right)-a\left({}^{n+1}\boldsymbol{z}^k,\overline{\boldsymbol{z}}\right)-b_N\left({}^{n+1}\boldsymbol{z}^k,\overline{\boldsymbol{z}}\right)\end{aligned} \tag{72}$$

4.2 Design Sensitivity Analysis of Frictionless Contact Problem

In the updated Lagrangian formulation, the reference frame is updated after each incremental analysis. Therefore, the design velocity field must also be updated after each incremental analysis on the updated reference frame. This update process can be obtained from the following relation

$${}^{n}\boldsymbol{x}={}^{0}\boldsymbol{x}+{}^{n}\boldsymbol{z} \tag{73}$$

By differentiating the relation of the above equation, the following design velocity update formula is obtained

$${}^{n}\boldsymbol{V}={}^{0}\boldsymbol{V}+{}^{n}\dot{\boldsymbol{z}} \tag{74}$$

Note that even when the initial design velocity field is given only to the die and punch, the design velocity field of a blank sheet is non-zero at the next time step.

The material derivative of the structural point on the slave surface at the current configuration becomes

$$\frac{d}{d\tau}{}^{n+1}\boldsymbol{x}_\tau\Big|_{\tau=0} = \frac{d}{d\tau}\left({}^{n}\boldsymbol{x}+\Delta\boldsymbol{z}\right)\Big|_{\tau=0} = {}^{n}\boldsymbol{V}+\Delta\dot{\boldsymbol{z}} \tag{75}$$

However, the material derivative of the contact point on the master surface is obtained using the chain rule and the material derivative of parametric coordinates as

$$\frac{d}{d\tau}{}^{n+1}\boldsymbol{x}^c_\tau\Big|_{\tau=0} = \boldsymbol{V}^c + \boldsymbol{e}_\alpha\dot{\xi}_\alpha \tag{76}$$

Since the master surface is assumed to be rigid, the initial velocity field calculated by perturbing the surface geometric matrix remains unchanged.
The material derivative of the contact variational form can be obtained as

$$\frac{d}{d\tau}b_N\left({}^{n+1}\boldsymbol{z},\overline{\boldsymbol{z}}\right)\Big|_{\tau=0} = \omega_n\int_{\Gamma^c}\left[\dot{g}\overline{g}+g\dot{\overline{g}}+gg\kappa V_n\right]d\Gamma \tag{77}$$

where κ is the curvature of the master surface, and V_n is the normal component of the design velocity. In the following, $\dot{g}$ and $\dot{\overline{g}}$ will be expressed with the implicit term $\Delta\dot{\boldsymbol{z}}$ and the explicit term ${}^{n}\boldsymbol{V}$. From its definition, the material derivative of the gap function can be obtained as

$$\dot{g} = \boldsymbol{n}\cdot\left(\Delta\dot{\boldsymbol{z}}+{}^{n}\hat{\boldsymbol{V}}\right) \tag{78}$$

where ${}^{n}\hat{\boldsymbol{V}} \equiv {}^{n}\boldsymbol{V}-\boldsymbol{V}^c$. However, the derivative of $\dot{\overline{g}}$ is not straightforward and the relation of $\overline{\boldsymbol{z}} = \overline{g}\boldsymbol{n}+g\overline{\boldsymbol{n}}+\boldsymbol{e}_\alpha\overline{\xi}_\alpha$ is needed to make the stiffness matrix symmetric Equation (78) thus becomes

$$\dot{\overline{g}} = -\left(\boldsymbol{n}\cdot\dot{\boldsymbol{e}}_\alpha\right)\overline{\xi}_\alpha + g\left(\boldsymbol{n}\cdot\dot{\boldsymbol{e}}_\alpha\right)m^{-1}_{\alpha\beta}\left(\boldsymbol{n}\cdot\overline{\boldsymbol{e}}_\beta\right) \tag{79}$$

where $\dot{\boldsymbol{e}}_\alpha = \boldsymbol{V}^c_{,\alpha} + {}^{n+1}\boldsymbol{x}^c_{,\alpha\beta}\dot{\xi}_\beta \equiv \boldsymbol{e}_\alpha\left(\Delta\dot{\boldsymbol{z}}\right)+\boldsymbol{e}_\alpha\left(\boldsymbol{V}\right)$ and $m_{\alpha\beta} = \boldsymbol{e}_\alpha\cdot\boldsymbol{e}_\beta$. The expression of $\dot{\xi}_\beta$ can be obtained from the consistency condition as

$$\begin{aligned}\dot{\xi}_\beta &= A^{-1}_{\alpha\beta}\left(\Delta\dot{\boldsymbol{z}}\cdot\boldsymbol{e}_\alpha\right)+A^{-1}_{\alpha\beta}\left({}^{n}\hat{\boldsymbol{V}}\cdot\boldsymbol{e}_\alpha+g\boldsymbol{n}\cdot\boldsymbol{V}^c_{,\alpha}\right)\\ &\equiv \xi_\beta\left(\Delta\dot{\boldsymbol{z}}\right)+\xi_\beta\left(\boldsymbol{V}\right)\end{aligned} \tag{80}$$

where $A_{\alpha\beta} = m_{\alpha\beta}-g\boldsymbol{n}\cdot{}^{n+1}\boldsymbol{x}^c_{,\alpha\beta}$. By using the relations from equations (78) to (80), the material derivative of the contact variational form can be separated into two parts, implicitly dependent and the explicitly dependent parts, as

$$\begin{aligned}&\frac{d}{d\tau}\left[b_N\left({}^{n+1}\boldsymbol{z},\overline{\boldsymbol{z}}\right)\right]\Big|_{\tau=0} =\\ &\quad b^*_N\left({}^{n+1}\boldsymbol{z};\Delta\dot{\boldsymbol{z}},\overline{\boldsymbol{z}}\right)+b'_N\left({}^{n+1}\boldsymbol{z};\boldsymbol{V},\overline{\boldsymbol{z}}\right)\end{aligned} \tag{81}$$

where

$$\begin{aligned}b^*_N\left({}^{n+1}\boldsymbol{z};\Delta\dot{\boldsymbol{z}},\overline{\boldsymbol{z}}\right) &= \omega_n\int_{{}^0\Gamma_c}\overline{\boldsymbol{z}}\cdot\boldsymbol{n}\boldsymbol{n}\cdot\Delta\dot{\boldsymbol{z}}d\Gamma\\ &-\omega_n\int_{{}^0\Gamma_c}g\left[\boldsymbol{n}\cdot{}^{n+1}\boldsymbol{x}^c_{,\alpha\beta}\overline{\xi}_\alpha\xi\left(\Delta\dot{\boldsymbol{z}}\right)\right]d\Gamma\\ &+\omega_n\int_{{}^0\Gamma_c}g^2\left[\left(n\cdot e_\alpha\left(\Delta\dot{\boldsymbol{z}}\right)\right)m^{-1}_{\alpha\beta}\left(\boldsymbol{n}\cdot\overline{\boldsymbol{e}}_\beta\right)\right]d\Gamma\end{aligned} \tag{82}$$

is the same form as the linearized contact bilinear form by substituting $\Delta\dot{\boldsymbol{z}}$ into $\Delta\boldsymbol{z}$, and the fictitious load terms is defined as

$$\begin{aligned}b'_N\left({}^{n+1}\boldsymbol{z};\boldsymbol{V},\overline{\boldsymbol{z}}\right) &\equiv b^*_N\left({}^{n+1}\boldsymbol{z};\boldsymbol{V},\overline{\boldsymbol{z}}\right)\\ &+\omega_n\int_{{}^0\Gamma_c}\left[\kappa g\overline{\boldsymbol{z}}\cdot\boldsymbol{n}V_n\right]d\Gamma\end{aligned} \tag{83}$$

5. NUMERICAL EXAMPLES

5.1 DSA of Pinched Hemisphere

A pinched hemispherical shell with an 18° hole at the top, under two inward and two outward forces 90° apart, as shown in Figure 2, is a frequent example for discussing shell structures. Because of symmetry conditions, only one quadrant is modeled. The material properties for this problem are Young's modulus, E=6.825×10^7, Poisson's ratio ν=0.3, radius R=10, and thickness t=0.04. The yield stress is σ_Y=2.43×10^5 and the hardening slope is H=3.0×10^5. A total of 289 meshfree particles are distributed in the structure, which corresponds to 1445 degrees-of-freedom.

DSA is carried out using the design velocity fields shown in Figure 3 with arrows. The computational cost of DSA per design parameter is about 3.1% of the response analysis cost, which is very efficient compared to the finite difference method.

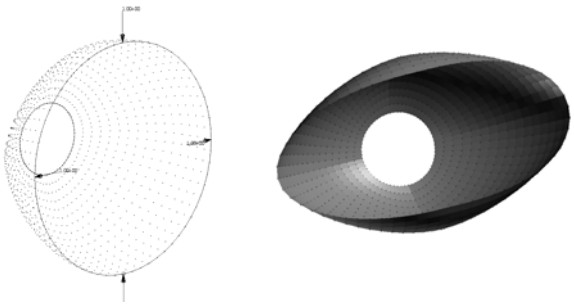

Figure 2. Pinched hemisphere

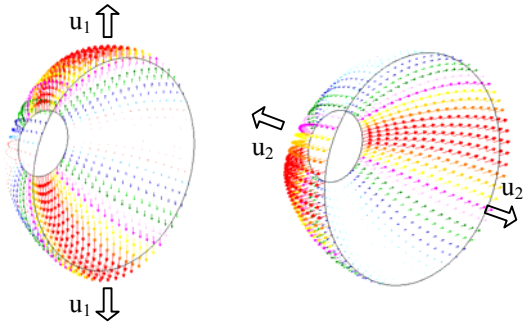

Figure 3. Design velocity fields: (a) u_1, (b) u_2.

Table 1. Accuracy of design sensitivity results

Design	Node	$\Delta\psi$	$\psi'\times\Delta\tau$	$(\Delta\psi/\psi'\Delta\tau)$ ×100
u_1	Z_1	3.8048E-3	3.8058E-3	99.97
	Z_{17}	-7.5058E-3	-7.5033E-3	100.03
	Z_{96}	5.2653E-4	5.2648E-4	100.01
	Z_{164}	4.3113E-4	4.3072E-4	100.10
	Z_{175}	-6.5461E-5	-6.5408E-5	100.08
	Z_{199}	3.4780E-4	3.4844E-4	99.82
u_2	Z_1	-1.3431E-3	-1.3427E-3	100.03
	Z_{17}	1.6425E-3	1.6426E-3	100.00
	Z_{96}	2.9782E-4	2.9778E-4	100.01
	Z_{164}	-4.7477E-5	-4.7482E-5	99.99
	Z_{175}	5.0661E-5	5.0696E-5	99.93
	Z_{199}	-1.5235E-5	-1.5336E-5	99.34

Displacement sensitivity results are compared with the finite difference results in Table 1, with excellent agreement. In Table 1, column $\Delta\psi$ is the finite difference result with perturbation size $\Delta\tau = 10^{-2}$, $\psi'\times\Delta\tau$ is the first-order approximation using the proposed sensitivity results, and the last column is the ratio between the finite difference and the proposed method.

5.2 DSA of Unconstrained Cylindrical Bending and Springback

The example of a blank sheet undergoing unconstrained cylindrical bending and springback is modeled to verify the proposed DSA method. As shown in Figure 4, the deformation is bending dominant and the springback after forming is large.

The radius of punch and die is 23.5 mm and the dimensions of the sheet are: 150 mm(L)×25 mm(W) ×1 mm(t). The punch and die are modeled as rigid. The material properties are Young's modulus, E=70 GPa, Poisson's ratio ν=0.34, yield stress σ_Y =184.3 MPa, and a hardening slope of 70 MPa. The total punch stroke is 25 mm.

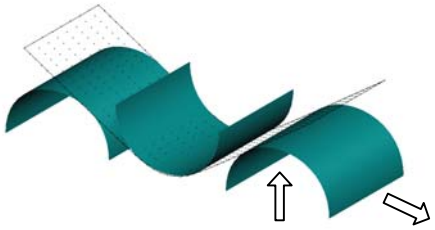

(a) Before springback

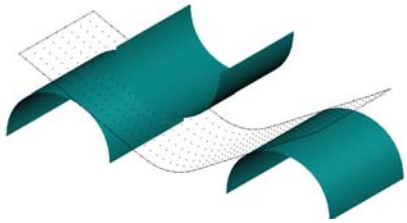

(b) After springback

Figure 4. Unconstrained cylindrical bending.

Table 2. Residual norm

Iteration	20% Stroke	100% Stroke	74% Stroke
2	1.30690E+02	4.48596E+02	8.70399E+00
3	2.45361E+02	4.49760E+01	1.01763E+00
4	1.97410E+02	1.17657E+00	6.71907E-01
5	3.16066E+01	1.31423E-02	1.89397E-02
6	8.36111E+01	1.79841E-07	5.57216E-07
7	3.78707E+00	3.16006E-11	6.86079E-13
8	1.56289E+00		
9	1.37232E-03		
10	1.70186E-07		
11	1.35113E-11		

The values of the residual norm during the typical Newton-Raphson iteration are shown in Table 2 at different punch locations. The result clearly shows a quadratic convergence.

DSA is carried out with horizontal and vertical locations of the right side die. as design variables as indicated in Figure 4.(a) with arrows. The computational cost of DSA per design parameter is about 14% of the response analysis cost. Vertical displacement sensitivity results are compared with finite difference results at different time steps in Table 2. The second column represents the punch location. For example, a 100% stroke corresponds to the configuration in Figure (a)

just before the punch goes up. The punch is completely separated from the blank sheet after a

Table 2. History of vertical displacement variation for DSA

Design	Stroke	Performance	ψ	$\Delta\psi$	$\psi'\times\Delta\tau$	$(\Delta\psi/\psi'\times\Delta\tau)\times100$
u_1	20%	z_{26}	4.02852E-04	1.55433E-05	1.55433E-05	100.00
		z_{29}	-5.63604E-04	1.09835E-06	1.09835E-06	100.00
		z_{35}	-2.11057E-03	2.74785E-07	2.74778E-07	100.00
		z_{45}	-1.18317E-03	-8.05724E-08	-8.05749E-08	100.00
	50%	z_{26}	5.17255E-03	1.56966E-06	1.57085E-06	99.92
		z_{29}	9.49035E-04	1.18913E-06	1.18945E-06	99.97
		z_{35}	-7.54700E-03	3.29706E-07	3.30085E-07	99.88
		z_{45}	-1.87226E-03	-1.75438E-10	-2.12434E-10	82.58
	80%	z_{26}	1.03687E-02	1.69248E-06	1.68963E-06	100.17
		z_{29}	2.64343E-03	1.20048E-06	1.16644E-06	100.09
		z_{35}	-1.26270E-02	2.77416E-07	2.77673E-07	99.91
		z_{45}	-2.49871E-03	-2.57553E-09	-2.56936E-09	100.24
	100%	z_{26}	1.34229E-02	1.50167E-06	1.49976E-06	100.13
		z_{29}	3.34870E-03	1.06836E-06	1.06806E-06	100.03
		z_{35}	-1.63456E-02	2.48267E-07	2.49360E-07	99.56
		z_{45}	-3.35510E-03	-1.53678E-09	-1.49009E-09	103.13
	74% (after springback)	z_{26}	9.07928E-03	1.67423E-06	1.67531E-06	99.94
		z_{29}	2.30504E-03	1.19530E-06	1.19633E-06	99.91
		z_{35}	-1.11233E-02	2.72550E-07	2.73327E-07	99.72
		z_{45}	-2.18794E-03	-6.57101E-09	-6.5414E-09	100.56
u_2	20%	z_{26}	4.02852E-04	-7.36074E-10	-7.07287E-10	104.07
		z_{29}	-5.63604E-04	-4.63381E-10	-4.43368E-10	104.51
		z_{35}	-2.11057E-03	-9.26439E-11	-8.77822E-11	105.54
		z_{45}	-1.18317E-03	-8.75209E-11	-8.82656E-11	99.16
	50%	z_{26}	5.17255E-03	-1.00382E-07	-9.99617E-08	100.42
		z_{29}	9.49035E-04	-1.76236E-07	-1.76003E-07	100.13
		z_{35}	-7.54700E-03	-1.09056E-07	-1.09054E-07	100.00
		z_{45}	-1.87226E-03	1.14161E-09	1.12875E-09	101.14
	80%	z_{26}	1.03687E-02	-8.0994E-07	-8.09024E-07	100.12
		z_{29}	2.64343E-03	-5.33790E-07	-5.33376E-07	100.08
		z_{35}	-1.26270E-02	-8.94977E-08	-8.92109E-08	100.32
		z_{45}	-2.49871E-03	2.31324E-09	2.29062E-09	100.99
	100%	z_{26}	1.34229E-02	-9.35092E-07	-9.34120E-07	100.10
		z_{29}	3.34870E-03	-6.10232E-07	-6.09977E-07	100.04
		z_{35}	-1.63456E-02	-9.34813E-08	-9.36087E-08	99.86
		z_{45}	-3.35510E-03	1.83968E-09	1.92688E-09	95.47
	74% (after springback)	z_{26}	9.07928E-03	-6.76509E-07	-6.76888E-07	99.94
		z_{29}	2.30504E-03	-4.61874E-07	-4.62311E-07	99.91
		z_{35}	-1.11233E-02	-7.31081E-08	-7.35101E-08	99.45
		z_{45}	-2.18794E-03	-2.45492E-08	-2.45808E-08	99.87

74% stroke. The ψ column provides displacement results. Some sensitivity results show inconsistency with finite difference results (i.e. z_{45} at 50% stroke with first design variable, and z_{26}, z_{29}, and z_{35} at 20% stroke). However, these discrepancies are due to insufficient numerical digits, and they disappear at the subsequent punch stroke.

6. CONCLUSION

A DSA method for the finite deformation elastoplastic shell structure with frictionless contact has been proposed. Since DSA uses the same tangent stiffness as analysis at the converged configuration of each time step, no iteration is required to solve the sensitivity equation. Consequently, DSA takes much less effort than nonlinear response analysis. The

accuracy and efficiency of sensitivity information is compared with finite difference results with excellent agreement.

7. ACKNOWLEDGEMENT

This research is supported by General Motors Corporation. This support is gratefully acknowledged.

8. REFERENCES

1. Kim, N.H., Choi, K.K., Chen, J.S., and Botkin, M.E., "Meshfree analysis and design sensitivity analysis for shell structures", International Journal of Numerical Methods in Engineering, Vol. 53, pp. 2087-2116, 2002.
2. Choi, B., Park, Y.H., Choi, K.K., "Shape design optimization of joining mechanism using doubly curved shell," Computers and Structures, Vol. 77, pp. 495-507, 2000.
3. Linby, T. Santos J.L.T., "Shape optimization of three-dimensional shell structures with the shape parameterization of a CAD system," Structural Optimization, Vol. 18, pp. 126-133, 1999.
4. Yamazaki, K., Vandeplaats, G.N., "Design sensitivity analysis with isoparametric shell elements," Structural Optimization, Vol. 5, pp. 152-158, 1993.
5. Moita, J.S., Barbosa, J.I., Soares, C.M.M., Soares, C.A.M., "Sensitivity analysis and optimal design of geometrically non-linear laminated plates and shells," Computers and Structures, Vol. 76, pp. 407-420, 2000.
6. Hughes, T.J.R. and Winget, J., "Finite rotation effects in numerical integration of rate constitutive equations arising in large deformation analysis", International Journal of Numerical Methods in Engineering, Vol. 15, pp. 1862-1867, 1980.
7. Hughes, T.J.R., "Numerical implementation of constitutive models: rate-independent deviatoric plasticity", *Theoretical Foundation for Large-scale Computations of Nonlinear Material Behavior*, Edited by Nemat-Nasser, S., Asaro, R.J., and Hegemier, G.A., Martinus Nijhoff Publishers, 1984.
8. Simo, J.C., Taylor, R.L., "A return mapping algorithm for plane stress elastoplasticity", International Journal of Numerical Methods in Engineering, Vol. 22, pp. 649-670, 2002.
9. Haug, E.J., Choi, K.K., and Komkov, V., *Design Sensitivity Analysis of Structural Systems*, Academic Press, New York, NY, 1986.
10. Fish, J. and Shek, K, "Computational aspect of incrementally objective algorithms for large deformation plasticity", International Journal of Numerical Methods in Engineering, Vol. 44, pp. 839-851, 1999.